JOURNAL OF MATERIALS SCIENCE 31 (1996) 6177–6184

# TEM study of the surface morphology of extracted $ZrO_2$–$Al_2O_3$ fibres

H. VALI, M. ALLAHVERDI*, R.A.L. DREW*
*Departments of Earth and Planetary Science and *Mining and Metallurgical Engineering, McGill University, 3450 University St, Montreal, Canada H3A 2A7*

The surface morphology and microstructure of a series of melt extracted $ZrO_2$–$Al_2O_3$ based fibres (ZA, ZAT and ZAS) have been imaged at the nanometre scale by transmission electron microscopy (TEM) using an advanced Pt/C replica technique. Growth characteristics of $ZrO_2$, $Al_2O_3$ and other crystalline phases formed upon heating up to 1550 °C are illustrated and described. Several grain morphologies including spherical and polygonal grains, as well as grains with rounded plate-like growth were observed indicating different active growth mechanisms. $ZrO_2$ particles on the surface of the fibres were almost spherical with some facetting and rounding of corners. These grains were very fine ($< 50$ nm) in the ZA and ZAS fibres while they were several microns in size in the ZAT fibres. $Al_2O_3$ grains were generally much larger (up to several microns) and exhibited two distinct growth morphologies of layered and rhombohedral type. Different grain morphologies of the ZA and ZAS fibres have been correlated to the phases identified by X-ray diffraction.

## 1. Introduction

Reactivity and physical properties of polycrystalline ceramics and related materials strongly depend on both surface topography and internal structure. In multiphase materials, a reliable characterization of microstructure involves the detailed analysis of size, shape, orientation, and distribution of grains as well as the relative amounts of each phase and the nature of the physical and chemical interactions of different phases present in the system. If the internal defects (e.g. dislocations), observed in most crystalline phases using transmission electron microscopy (TEM), are considered as growth phenomena, then, it is most likely that related microtopographic features, at the same scale, will also be present on the cleavage and as-grown surfaces of individual crystals. Thus, it is important to correlate internal and surface structures at the TEM scale.

The surface morphology of crystalline material is conventionally investigated by scanning electron microscopy (SEM) and by atomic force microscopy (AFM). However, the resolution limit of SEM does not permit the detection of morphological features at a fine scale. With AFM, the surface structure of a crystal can be studied at near atomic resolution. In most cases, AFM is applied to *in situ* investigations of smooth surfaces. AFM is not suitable for investigation of fragments having rough and irregular topography. An alternative technique is imaging replicas using TEM. Replicas are prepared by condensation of heavy metals (e.g. Au, Ag, and Pt) on as-grown, as-made, or fractured surfaces. This "decoration and shadowing" technique offers a unique opportunity to investigate the detailed characteristics of surface morphologies with considerable resolution. Investigations of the surface morphology of crystals can be made at a resolution near 1 nm. Correlation between the internal and surface structures at the same scale is also possible.

Decoration and shadowing techniques have become a valuable tool to study the topomorphology and topochemistry of biological specimens. This technique was also among the earliest methods employed in TEM studies. Cleavage surfaces of inorganic substrates (e.g. sodium chloride) have been studied to characterize both surface imperfections on crystals and mechanisms of nucleation and growth of metal thin films [1, 2]. Surface microtopography and growth mechanisms of layered silicates were also studied using decoration and shadowing techniques [3–6]. Since the nucleation and formation of evaporated metal clusters depend, among other parameters, on the nature of crystal surface (e.g. chemical affinity, binding energy and hydration state), a careful interpretation of a replica, obtained by decoration and shadowing method, can provide significant information concerning growth evolution of crystals.

## 2. Experimental procedure

A series of heat-treated, fine polycrystalline oxide fibres were selected in order to study the characteristics of surface microstructures. These oxide fibres were initially produced as amorphous (or slightly crystalline, $< 5\%$) by a melt extraction technique [7–10]. The initial composition of the oxide systems used are listed in Table I. These oxides are based on $ZrO_2$–$Al_2O_3$ with the addition of silica and titania,

0022–2461  

TABLE I Chemical compositions of the three oxide systems studied

| Oxide compound | $ZrO_2$ (wt %) (mol %) | $Al_2O_3$ (wt %) (mol %) | $SiO_2$ (wt %) (mol %) | $TiO_2$ (wt %) (mol %) |
|---|---|---|---|---|
| $ZrO_2$–$Al_2O_3$ (ZA) | 42.6 (38) | 57.4 (62) | – | – |
| $ZrO_2$–$Al_2O_3$–$TiO_2$ (ZAT) | 44 (37.8) | 42 (43.6) | – | 14 (18.6) |
| $ZrO_2$–$Al_2O_3$–$SiO_2$ (ZAS) | 31 (24.3) | 53 (50) | 16 (25.7) | – |

and the resulting fibres are referred to as ZA, ZAS and ZAT, respectively.

A bundle of the extracted fibres was placed in a furnace at room temperature, heated up to a desired temperature in air, and held for one hour. The heat-treated fibres were then cooled to room temperature inside the furnace. Since there were limited amounts of sample available, the fibres were subsequently heat-treated above the crystallization temperatures of the fibres at 1000, 1100, 1250, 1400 and 1550 °C [9]. For purpose of this study, we will mainly focus on a series of samples heated up to 1550 °C. The results obtained from ion-milled samples will be also used, to a limited extent, to explain the surface characteristics of the fibres.

## 2.1. Platinum/Carbon Replicas

The surface microtopography of individual fibres was examined on high-resolution replicas by TEM. The replicas consist of a thin platinum/carbon (Pt/C) film (95Pt/5C wt % and 1–2 nm thick) and a supporting carbon film (15–20 nm thick). Individual fibres were mounted on a flat substrate using double-sided adhesive tape, with the surface of interest parallel to the substrate. The shadowing and replication procedure was performed in a freeze–etch unit (Balzer 400) under high vacuum ($1.333 \times 10^{-4}$ Pa) and at room temperature. An extremely fine granular Pt/C film was condensed on the crystal surface by an electron beam evaporation gun as a point source at an angle of 30° and a distance of 15 cm. Instrumental conditions (i.e. acceleration potential and emission current) allowed a Pt/C deposition rate of 0.25 nm $s^{-1}$. The thickness of the metal film was determined by measuring the frequency shift of a quartz crystal thin film oscillator that was mounted as close as possible to the object. The centring rod of the evaporation gun was pointed halfway between the quartz and specimen holder. In cases where the orientation of the quartz crystal and the object were the same (with respect to the angle of incident beam), the actual thickness of the metal film was compared directly with that measured by the quartz monitor. However, a more accurate thickness of the metal film was assessed by positioning the quartz crystal perpendicular to the direction of incident flux of Pt/C atoms. By knowing the oblique angle of the gun with respect to the specimen stage, the actual deposition rate and thickness of the metal film on the sample surface were calculated.

A supporting carbon film was immediately condensed on the Pt/C coating by a vertical electron beam gun at 90° at 12 cm distance away from the surface of the specimen for 6 seconds. Under the optimal operational conditions and a deposition rate of 2.5 nm $s^{-1}$, a total thickness of $\approx 15$ nm carbon film was produced. The replica was cleaned by dissolving the fibres adhering to the replica with a 10% HF solution, rinsed with deionized water and transferred onto 200 mesh TEM grids.

## 2.2. Ion-milled thin sections

In order to image the internal structure of the fibres, samples were prepared by ion beam milling (Dual Ion Mill, model 600 Gatan Inc., USA). Ceramic fibres were initially placed and glued to a copper grid using a special low viscosity resin and then ion milled for several hours at 6 kV, 0.5 mA and an incident beam angle of 15°. A thin carbon film was then deposited on the thinned sections to avoid charging problem and enhancing the resolution of TEM images.

TEM imaging was performed with a Jeol 100 CX equipped with an energy-dispersive X-ray (EDX) detector (PGT IV, analysable area $\approx 100$ nm$^2$) at an accelerating voltage of 100 kV with imaging conditions of underfocus.

## 3. Results and discussion

Fig. 1 represents the surface microstructure of the ZA sample heated to 1550 °C. According to the X-ray results (Table II), $\alpha$-$Al_2O_3$ (rhombohedral alumina) and t-$ZrO_2$ (tetragonal zirconia) are the two predominant phases present in this sample.

The TEM images revealed the presence of large $Al_2O_3$ crystals displaying at least two distinct morphologies. One appears as anhedral, layered crystals (marked A in Fig. 1a) with rounded growth steps which mimics the operation of a spiral growth mechanism. However, the thicknesses of the layers (arrows in Fig. 1a) are much larger than the height of the individual lattice planes. The second type exhibits an euhedral, rhombohedral crystal shape with numerous outcropping screw dislocation patterns showing rational, equivalent crystal faces (arrows in Fig. 1b). Since, the habit and surface structure of a crystal reflect the conditions of crystallization (e.g. chemical composition and temperature), the coexistence of two distinct crystal shapes within the sample, even as adjacent grains, indicates changes in physical and/or chemical gradients within the system at a nanometre scale. McKittrick *et al.* [11] have reported changes in $ZrO_2/Al_2O_3$ ratios upon heating. They have documented that the $\alpha$-$Al_2O_3$ phase contains less $ZrO_2$ than the $\delta$-$Al_2O_3$ phase and concluded that $ZrO_2$ has limited solubility in $\alpha$-$Al_2O_3$. However, since the present materials are produced by sequential reheating of the amorphous fibres, differences in crystal habits could also be a result of physical factors such as temperature and the kinetics of crystallization and reaction. It is important to mention that the proportion of the layered, plate-like crystals is much less in the samples heat treated at lower temperatures.

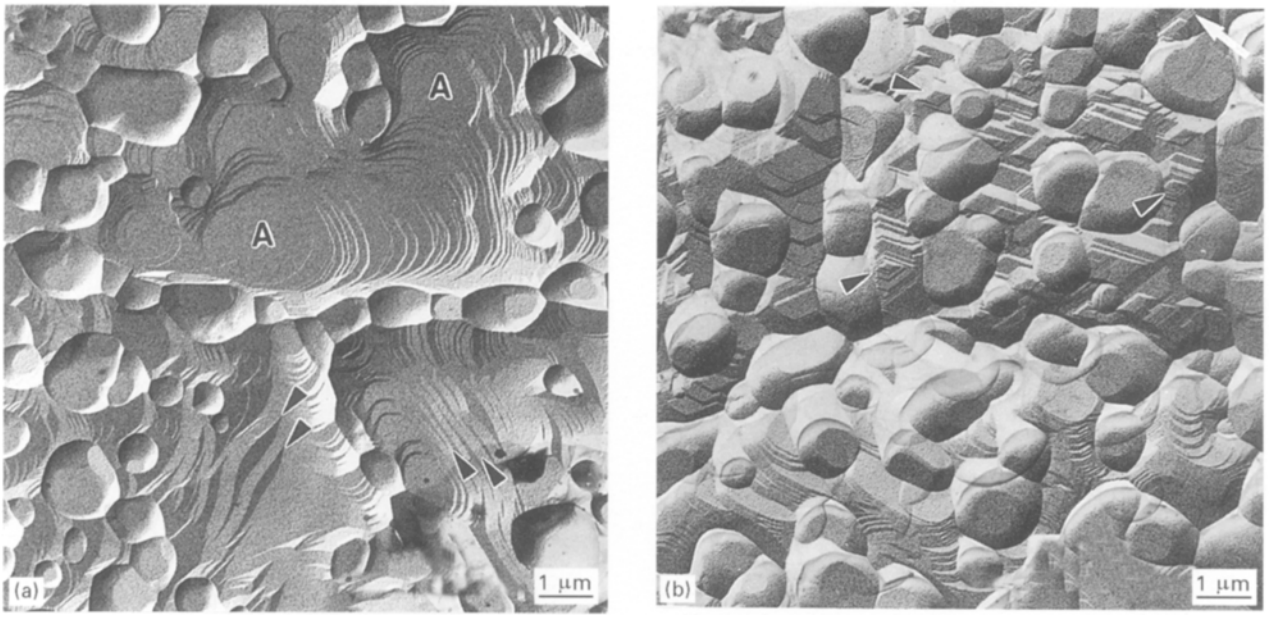


*Figure 1* TEM images or Pt/C replicas obtained from the surface of ZA fibres heated to 1550 °C. (a) Stable α-alumina grains with rounded plate-like growth are denoted by "A". Arrows show the growth steps of these grains. Zirconia particles are either within alumina grains or lined up at grain boundaries. (b) Alumina crystals with outcropping screw dislocations (see arrows). White arrow in the upper right shows the shadowing direction.

TABLE II Phase analysis of the fibres heat treated to the final temperature of 1550 °C

| Fibre | Phases identified |
|---|---|
| ZA | t-$ZrO_2$ and α-$Al_2O_3$ |
| ZAT | [t-$ZrO_2$, m-$ZrO_2$], α-$Al_2O_3$, $ZrTiO_4$ and $Al_2TiO_5$ |
| ZAS | t-$ZrO_2$, α-$Al_2O_3$ and mullite |

$ZrO_2$ was present as individual particles dispersed within the $Al_2O_3$ grains or as chain-like aggregates (Fig. 1a) lining up along the grain boundaries of $Al_2O_3$ phase. A wide range of particle size (50–500 nm) can be observed for the $ZrO_2$ particles. Smaller crystals occurred as spheres, while larger crystals appeared as pseudo-prismatic grains consisting of flat crystal faces with rounded edges and corners (Fig. 1). If the flat surfaces of $ZrO_2$ grains represent a crystallographic face (e.g. one of the tetragonal faces), then all grains exhibiting their flat faces parallel to the fibre surface must have the same crystallographic orientation. Crystals located along the boundaries display a stronger deformation than isolated $ZrO_2$ grains (Fig. 1a). Modification of these grains is a result of interaction between two or more $ZrO_2$ grains (leading to coarsening) and the interaction between $ZrO_2$ and $Al_2O_3$ phases. However, it remains unclear whether the formation and arrangement of these grains along the boundaries are related to primary nucleation and growth of $ZrO_2$, or are a consequence of secondary crystallization of $ZrO_2$ from supersaturated $Al_2O_3$ phase. It is well documented [11–14] that in the devitrification of glassy eutectic $Al_2O_3$–$ZrO_2$, the first precipitated $Al_2O_3$ phases (γ, ε and δ-$Al_2O_3$) incorporate a large amount of $ZrO_2$. In contrast, α-$Al_2O_3$, which forms at higher annealing temperatures ( > 1200 °C), contains much less $ZrO_2$. Since the only $Al_2O_3$ phase detected in the present sample was α-$Al_2O_3$, it is most likely that the $ZrO_2$ particles at the grain boundaries formed during the conversion of metastable $Al_2O_3$ to the stable α-form during heating. This hypothesis is supported by the fact that the samples heat treated at a lower temperature (1250 °C) did not show any accumulation of $ZrO_2$ particles along the $Al_2O_3$ boundaries [9].

Evidence of $ZrO_2$ particle contact, which would eventually lead to neck growth and grain coalescence, can also be observed (Fig. 1). An ion-milled specimen obtained from the heat treated fibres at 1400 °C revealed, in most cases, the presence of an interface at the contact of the grains. This interface was eliminated only in a few cases. Since heat-treated fibres at 1250 °C revealed much smaller $ZrO_2$ grains with more prismatic morphology and a more uniform distribution within the $Al_2O_3$ matrix, it is evident that extensive rearrangement, coarsening and spherodization of both $ZrO_2$ and $Al_2O_3$ crystals have occurred upon heating at 1400 and 1550 °C. However, the grain size of $ZrO_2$ ( < 100 nm at 1400 °C) seems to be much smaller than that reported by McKittrick *et al.* [11] for a pure $Al_2O_3$–$ZrO_2$ eutectic system (i.e. a few hundred nm at 1450 °C). In addition, these authors only found evidence of a monoclinic polymorph of $ZrO_2$ in their samples. Tetragonal $ZrO_2$ was the only polymorph found in the present fibres even after heat treatment at 1550 °C. This discrepancy can be explained by the fact that the $ZrO_2$ used in the present study contains 3 mol % $Y_2O_3$, which would inhibit the transformation of tetragonal to monoclinic, particularly at the fine scale observed in these micrographs.

Fig. 2 shows the surface structure of heat treated ZAT fibres at 1550 °C. In contrast to ZA, there is

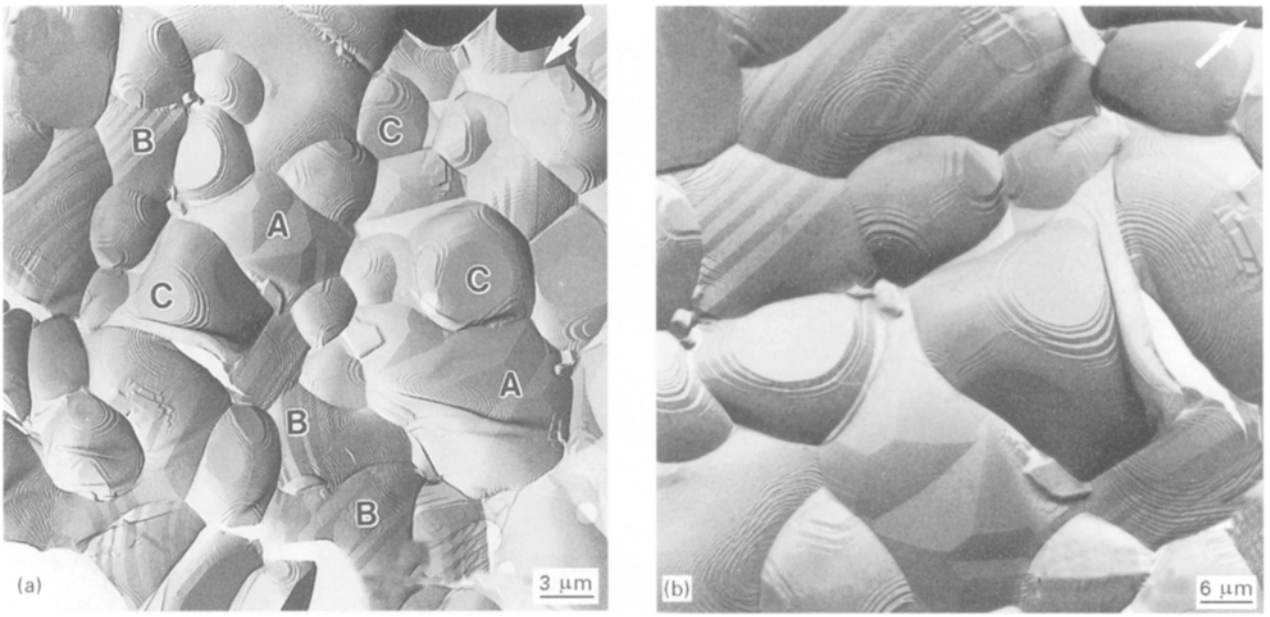


*Figure 2* TEM images or Pt/C replicas obtained from the surface of the ZAT fibres heated to 1550 °C. (a) Three types of grains can be distinguished: (i) prismatic crystals with flat surfaces and sharp edges (A), (ii) grains with step-like, terraced surface (B), and (iii) polygonal grains with rounded steps characteristics of spiral growth (C). (b) Higher magnification of (a) indicating the detail characteristics of surface. White arrow in the upper right shows the shadowing direction.

a significant difference in the microstructure along the longitudinal axis of the fibres. The most common feature of this sample is the growth of almost spherical particles (Fig. 2). Some regions of the fibres showed a combination of elongated and spherical particles. In general, compared to the ZA samples, an accurate interpretation of the surface morphology of this material is more difficult. X-ray analysis of the ZAT fibres revealed the presence of five distinct phases when heated to 1550 °C (see Table II). $ZrO_2$ occurred in both monoclinic and tetragonal modifications, while $\alpha$-$Al_2O_3$ was the only detectable $Al_2O_3$ phase. $ZrTiO_4$ and $Al_2TiO_5$ phases were also identified. However, a direct correlation of these different phases to the individual grains, observed on the TEM images, was not possible.

In Fig. 2, three types of grains with distinct surface structures could be recognized. The first type was a prismatic crystal with perfectly developed flat faces and sharp edges (marked A in Fig. 2a). The second type displayed a step-like, terraced surface (marked B in Fig. 2a). In Pt/C replicas, the surface of these crystals mimics a lamellar-like texture consisting of alternating dark and bright contrast. However, the apparent contrast differences on the TEM images is a result of variation in the rate of Pt/C deposition on the fibres having different angular orientation with respect to the incident flux of Pt/C atoms. The highest deposition rate (dark contrast in Fig. 2) is excepted at 90°, and the lowest at angles $< 10°$. Therefore, lamellae displaying dark contrast correspond to vertical crystal faces (step heights) and lamellae with brighter contrast represent the horizontal face (step separation). A similar lamellar structure was also observed in the ion milled specimens heat treated at 1400 °C (arrows in Fig. 3a). This feature was associated with a component that occurred as both individual particles surrounded by $\alpha$-$Al_2O_3$ and also as a continuous matrix at the grain boundaries. AEM (analytical electron microscopy) analysis of this component revealed the presence of Zr, Ti and small amounts of Al. It is most likely that this phase corresponds to the $ZrTiO_4$ phase detected by X-ray analysis of this sample (Table II). Similar modulated structures have been reported from a monoclinic $ZrO_2$ formed during the heat treatment of eutectic $Al_2O_3$–$ZrO_2$ glasses at 1450 °C [11]. Stevens [15] reported the formation of a lamellar structure in pure $ZrO_2$ as a result of tetragonal to monoclinic phase transformation (at 900–1100 °C). Extensive modulation of plate-like domains have also been observed in $ZrO_2$–$Y_2O_3$ system by the cubic to tetragonal [16], and by tetragonal to monoclinic [17] transformations of $ZrO_2$.

Note that while the tetragonal to monoclinic transformation of $ZrO_2$ occurred in the ZAT fibres, it was not observed after heat treatment of the ZA sample at 1550 °C. The particle size of $ZrO_2$ in the ZA fibres is much smaller than that reported in the above studies. This discrepancy may be explained by the fact that tetragonal to monoclinic transformation is also a function of grain size [18].

The third type of grains in the ZAT fibres is a polygonal crystal having two distinct faces (marked C in Fig. 2a); a flat surface with no growth pattern, and a face with rounded steps, characteristic of spiral growth. It is most likely that these grains correspond to the tetragonal $ZrO_2$ found by X-ray diffraction. However, there was no clear evidence for the presence of pure $ZrO_2$ in this sample. Microanalysis of ion-milled specimens revealed the presence of Ti, associated with Zr and/or Al, in most of the grains, with the exception of $\alpha$-$Al_2O_3$. This suggests the occurrence of a variety of solid solution phases among the $Al_2O_3$, $ZrO_2$, and $TiO_2$ end-members. Compared with the

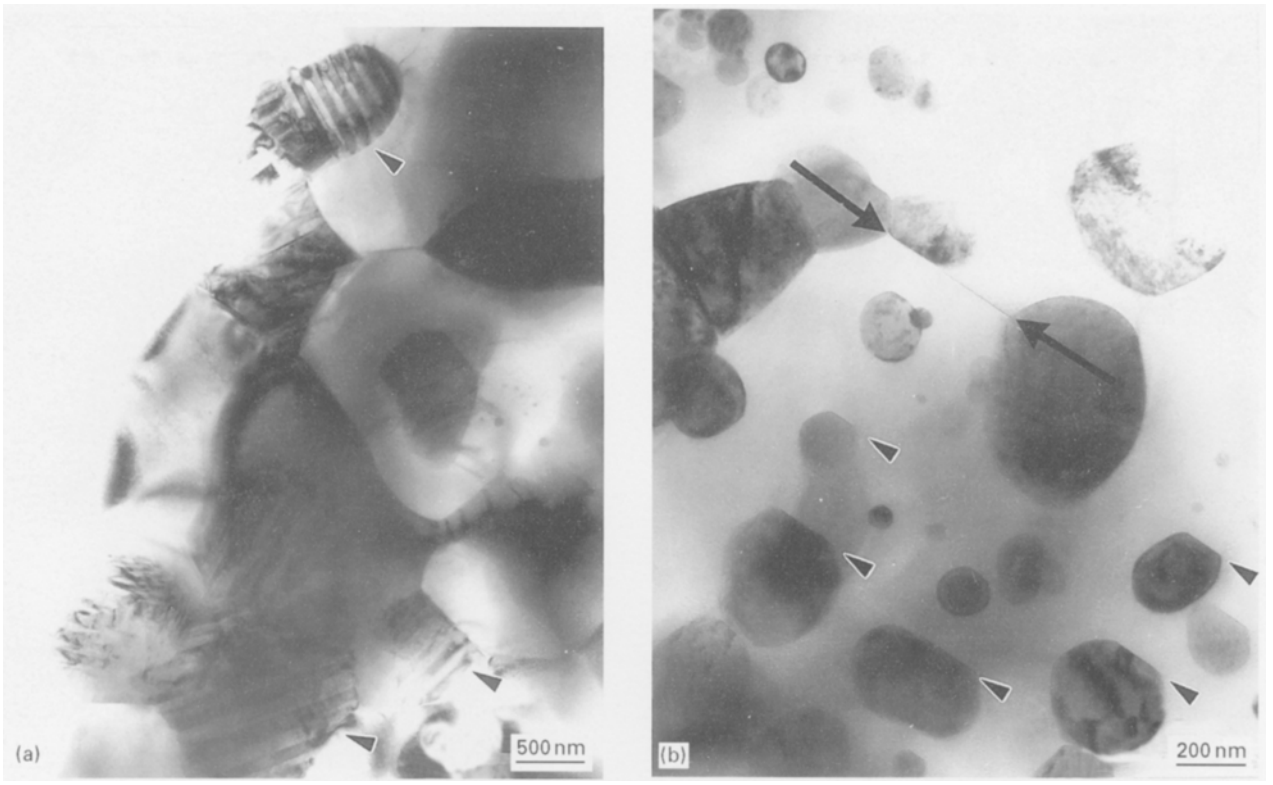


*Figure 3* (a) Ion milled thin section of the ZAT fibre heated up to 1400 °C. Step-like terraced grains (arrows), shown previously (Fig. 2a), can also be seen within the fibres even at a lower heat treatment temperature. (b) Internal structure of the ZAS fibre heated up to 1400 °C. Note the variation in zirconia particle size (dark grey particles) and also the straight edges of these particles (small arrows) which exhibit the same orientation. These edges are all parallel to the grain boundary (large arrows) indicating the crystallographic relationship between zirconia particles and the matrix.

samples heat-treated at lower temperatures (e.g. 1250 °C), extensive rearrangement of grains has occurred. Distinction between primary and secondary recrystallizations of the individual phases formed at 1550 °C could not be made. The development of grain boundaries, the mechanisms of growth, and the coarsening of distinct phases involved in this system could not be recognized. The nature of the grain boundary in the ZAT fibres is much more complicated than for the ZA material. Fig. 2 indicates coalescence of grains with both curved and flat boundaries. If the general rule of movement of a boundary toward the centre of curvature can be applied to these samples, then it may be possible to assess the development of microstructure in term of grain growth and coarsening by studying the characteristics of the grain boundaries.

Fig. 4 shows the surface morphology of the ZAS fibres heat treated at 1550 °C. According to the X-ray results (Table II), this sample consists of t-$ZrO_2$, $\alpha$-$Al_2O_3$ and mullite phases. In TEM images of Pt/C replicas, three distinct types of crystals were observed. Similar to ZA fibres, $ZrO_2$ was characterized by its spherical grain morphology with one or more flat surfaces (Fig. 4a, b). $\alpha$-$Al_2O_3$ was present as plate-like crystals with rounded edges mimicking the operation of a spiral growth mechanism (arrows in Fig. 4a). Elongated, prismatic crystals with a layered surface structure may represent the mullite phase (Fig. 4a, centre). Elongated mullite grains with high aspect ratios were reported previously [19, 20] when mullite bodies were prepared through sol–gel methods. In contrast to the ZAT fibres, these three phases were also present in the heat-treated fibres at lower temperatures. However, extensive changes in the microstructure (i.e. surface morphology, dimensions and distribution of individual phases) have occurred after heat treatment at 1550 °C.

Fig. 4b shows the growth patterns of one of the prismatic crystals associated with $ZrO_2$. Although a clear interpretation of the surface structure appears to be very difficult, there are distinct crystallographically rational faces having the same orientation. To describe the growth characteristics of different types of faces present on this crystal, crystal symmetry and orientation of the crystal axes must be determined. Since both $Al_2O_3$ (hexagonal) and mullite (orthorhombic) form prismatic crystals, an attempt was made to find criteria which would help to locate the crystal symmetry. There are several dislocation sites present on the surface, shown in Fig. 4b, that are characterized by flat faces (F), equivalent stepped faces (S), and smooth prismatic faces (X and O). The angle between prismatic and flat faces appears to be at right angles. The angle between equivalent S-faces also seem to be closer to 90° rather than 60° or 120° as shown in Fig. 1b for $\alpha$-$Al_2O_3$. In addition, the overall elongated shape of these crystals at lower magnification indicates more of a similarity to a mullite rather than an $Al_2O_3$ phase. However, the accurate identification of crystal structure requires additional information (e.g. X-ray, EDX, and ion milling). Rice [21] has shown a SEM image of a fractured surface of a solidified $Al_2O_3$–$ZrO_2$ specimen, indicating the development of

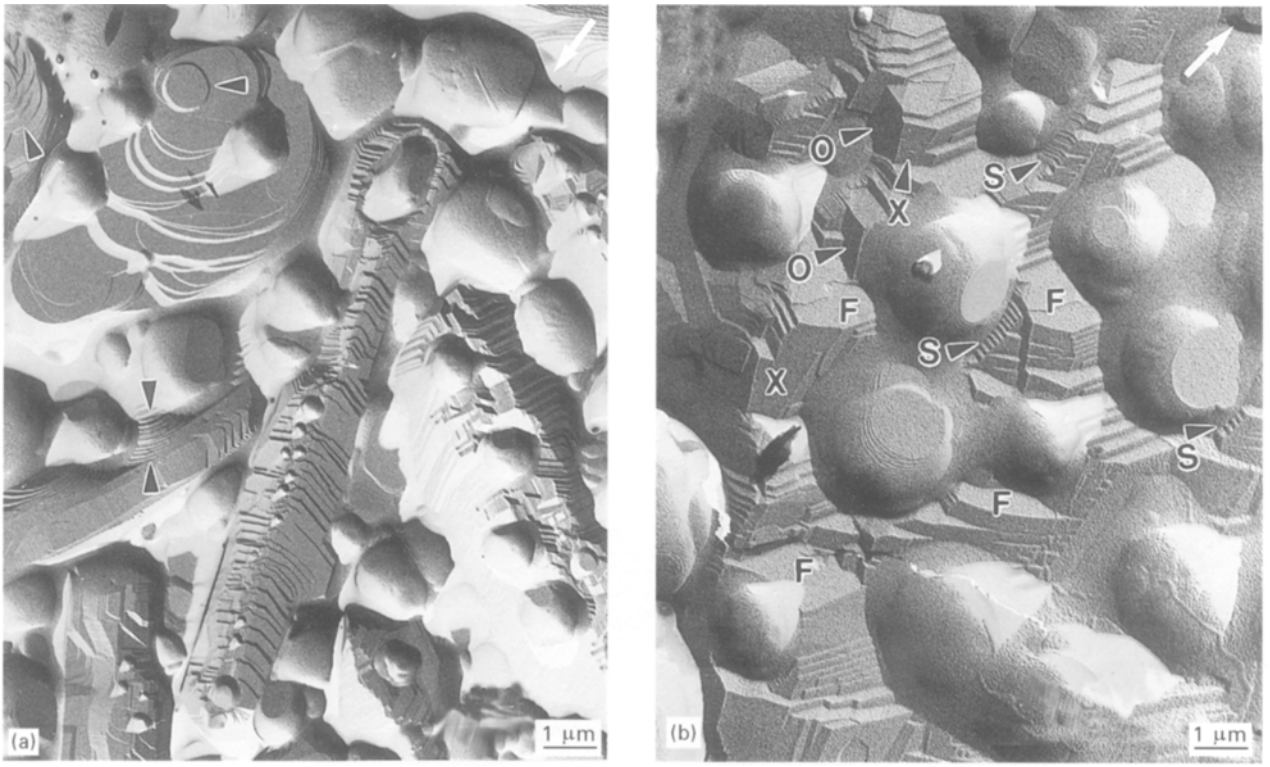


*Figure 4* TEM images or Pt/C replicas obtained from the surface of ZAS fibres heated up to 1550 °C. (a) α-alumina exhibit plate like growth with rounded edges (arrows). Large elongated prismatic crystal in the centre of micrograph may represent a mullite grain. Rounded particles with submicron to micron size are zirconia particles. (b) Growth pattern of a prismatic grain on the surface of a ZAS fibre. Different faces of flat (F), stepped (S), and smooth prismatic (X and O) are shown. Zirconia particles are rounded particles and are surrounded by a glassy phase. White arrow in the upper right shows the shadowing direction.

a complex microtopography. Similar features have been observed in the present study. Nevertheless, the development of such complicated crystal facets suggests extensive variations in physical and/or chemical gradients controlling the growth rates of individual faces.

Similar to ZA fibres, particles of $ZrO_2$ in the ZAS were recognized by their spherical crystals shape having at least one flat face. As shown in Fig. 4a, there were extensive variations in particle size of $ZrO_2$ ranging from a few tens to a few hundreds of nanometres. Smaller particles were associated predominately with mullite whereas larger particles were mostly present at grain boundaries. This is also evident on ion-milled specimens of the heat treated fibres at 1400 °C (Fig. 3b). The heat-treated fibres at 1250 °C revealed a more homogeneous size distribution of $ZrO_2$ crystals having more polygonal shape. Therefore, it is concluded that spherical $ZrO_2$ inclusions within the mullite and $Al_2O_3$ crystals have formed during the subsequent heat treatment at 1400 °C. Note that some of the grains in Fig. 3b seem to have the same orientation. The straight edges of these crystals (small arrows in Fig. 3b) are also parallel to the grain boundary of the matrix (large arrows in Fig. 3b). This indicates a crystallographic correlation of these grains with the matrix.

Crystallization of secondary $ZrO_2$ is also associated with the coarsening and phase transformation of $Al_2O_3$ which also takes place in our experiments within the same temperature range. According to McKittrick *et al.* [11, 13], $ZrO_2$ is much less soluble in $\alpha$-$Al_2O_3$ than in $\gamma, \varepsilon$ or $\delta$-$Al_2O_3$ which are supersaturated with respect to $ZrO_2$. If so, it is most likely that the small $ZrO_2$ particles present within the $\alpha$-$Al_2O_3$ and mullite crystals nucleated as a result of solute rejection ($ZrO_2$) during phase transformation of $Al_2O_3$ which occurs at temperatures of $> 1250$ °C for this material [9].

It is important to mention that the heat treatment at 1550 °C resulted in extensive changes in the surface morphology, particularly with respect to the distribution of $ZrO_2$ within the mullite and $Al_2O_3$ phases. The amount of small $ZrO_2$ particles associated with $Al_2O_3$ and mullite phases decreased considerably compared to the fibres heat-treated at 1400 °C. Simultaneous coarsening of $ZrO_2$ grains and growth of the unique crystallographic facets in $Al_2O_3$ and mullite crystals (Fig. 4) suggest an extensive recrystallization of fibres at 1550 °C. It is most likely that the coarsening of $ZrO_2$ within the $Al_2O_3$ and mullite resulted from the movement of small $ZrO_2$ inclusions at high temperatures [22].

It was observed that the surface of the heat-treated ZAS fibres at 1400 °C was covered with an amorphous material surrounding $ZrO_2$ particles which is probably $SiO_2$ rich. Upon heating to 1550 °C, most of this material disappeared. Since the reduction of this glass is associated with the development of growth facets of the phases described above, it is assumed that this material is a residue of the initial amorphous matrix in ZAS fibres produced during melt extraction. As shown in Fig. 4b, the remaining proportion of this glassy material is accumulated around the $ZrO_2$ grains.

Association of this "amorphous" phase with $ZrO_2$ suggests an active chemical interaction at the interface between these two phases. Such a feature on the surface may be characteristic of an incomplete reaction in terms of temperature and duration of heat treatment [22]. This feature was only observed in ZAS samples and is typical of devitrification of silicate materials.

In the course of subsequent heat treatment (1000, 1100, 1250, 1400 and 1550 °C) of rapidly solidified amorphous fibres, several metastable, non-equilibrium solid solution phases have formed at lower temperatures. With increasing temperature, some of these metastable phases disappeared or converted to more stable phases. At 1550 °C, almost pure $\alpha$-$Al_2O_3$ was found in all samples as the stable $Al_2O_3$ polymorph, while pure $ZrO_2$ (containing small amounts of $Y_2O_3$) was found in the ZA system only. In the ZA system, there are some discrepancies between the current results and the data available in the literature (discussed above) with respect to phase transformation, crystal growth, and microstructure at various temperatures. In general, the grain size of $ZrO_2$ was always smaller, at a given temperature, in the present samples. No evidence of monoclinic $ZrO_2$ phase was found in our samples with the exception of ZAT fibres at 1550 °C. It is likely that some $Y_2O_3$ might have been retained in the $ZrO_2$ grains of ZAT fibres causing monoclinic polymorph to form (during cooling to room temperature), or the size factor of $ZrO_2$ grains might have caused the formation of monoclinic $ZrO_2$.

The TEM images, described above, reflect the predominant microstructures observed in the fibres obtained from the ZA, ZAT and ZAS systems. In some cases, however, there were extensive variations in the surface morphology with respect to the size, shape, distribution and arrangement of grains. It is likely that non-uniformity of the rapidly solidified, glassy fibres results in the formation of a material having a heterogeneous composition at a very fine scale. The local variations in internal structure and surface morphology of the heat treated fibres, therefore, may reflect regional heterogeneities in the chemical compositions of the extracted fibres at a micro scale.

Since experimental conditions for all samples were the same, it is evident that the chemical composition of the starting material controls the nucleation and growth patterns of individual phases. To interpret the growth characteristics of the individual phases, an attempt is made to predict the nature of reaction and the mechanism of crystal growth at the surface. In general, thermodynamic calculations and modelling have been applied to predict the growth characteristics in crystals growing from liquid, vapour, or solid phases. The reaction of the interface between a growing solid phase and the surrounding medium determines the mechanism of growth. It is assumed that, in the case of anhedral crystals having rounded faces, a continuous growth mechanism operates at the interface. Euhedral crystals having a smooth surface and crystallographic rational faces are grown by a layer-spreading mechanism. In most cases, the layer-spreading processes are associated with spiral growth and/or surface nucleation growth mechanisms [24]. Depending on the numbers and arrangements of periodic bond chains (PBCs) [25, 26] three types of faces can develop during crystal growth. Growth slices containing two PBCs are classified as flat faces (F). Stepped faces (S) contain one PBC and kinked faces (K) contain no PBCs. Any departure from equilibrium results in the occurrence of different types of faces in an individual crystal (e.g. $ZrO_2$). Selective incorporation of impurities (trace elements) on distinct crystallographic sites are responsible for the development of a variety of facets (preferential growth on distinct crystal faces) in a single crystal. Growth of S and K faces is also associated with partitioning of trace elements.

The extensive diversity in growth features, observed on TEM images of high resolution Pt/C replicas, offers a unique opportunity to study the growth characteristics of real crystals. Although the formation of all types of faces, described above, are evident in our samples, polycrystalline and multiphase nature of the systems studied makes it difficult to establish an accurate correlation between the theoretical models and experimental results. It is most likely that the surface structures of the fibres have been developed by a combination of solid state diffusion and interfacial reactions between the vapour and solid phase. If the traditional thermodynamics and growth rules can be applied to our materials, then the growth patterns, observed on individual grains and crystalline matrix, suggest a non-equilibrium crystallization for all phases involved. The most reasonable assumption for this phenomenon is partitioning of trace element within the structure of endmember phases (e.g. $\alpha$-$Al_2O_3$ and t-$ZrO_2$) or the formation of non-stoichiometric solid solution at non-equilibrium conditions. However, there are many other factors influencing the microstructure of these very complicated systems which are not discussed here. A simple monophasic system may be more suitable for the study of crystal growth.

This study is the first attempt in using replica techniques to image the growth pattern of oxide ceramic fibres heat treated at elevated temperatures. The most significant achievement of the present work is the capability of correlating the surface microtopography with the internal structure.

## 4. Conclusions

This study is the first report on detailed surface morphology of a series of new type of $Al_2O_3$–$ZrO_2$ based fibres produced by a novel melt extraction technique. The following conclusions can be drawn:

1. The application of high resolution Pt/C replica enables a correlation of internal and surface structures at the TEM scale.
2. The growth characteristics of individual phases can be studied at the nanometre scale, and involves the development of various crystal faces and facets.
3. Using this technique, it is possible to correlate thermodynamic modelling with the observed growth

characteristics of crystals growing during the devitrification of amorphous materials.

## References


1. G. BASSETT, *Phil. Mag.* **3** (1958) 1042.
2. H. BETHGE and J. HEYDENREICH (eds) "Electron Microscopy in Solid Physics" (Elsevier, Amsterdam, 1987).
3. A. BARONNET, *Amer. Mineralog.* **57** (1972) 1272.
4. A. BARONNET, in "Minerals and reactions at atomic scale: transmission electron microscopy", edited by P. R. Buseck (Mineralogical Society of America, Washington, DC, 1992), p. 231.
5. S. TOMURA, M. KITAMURA and I. SUNGAWA, *Phys. Chem. Min.* **5** (1979) 65.
6. H. VALI, R. HESSE and E.E. KOHLER, *Amer. Mineralog.* **76** (1991) 1973.
7. M. ALLAHVERDI, R. A. L. DREW and J. STROM OLSEN, *J. Mater. Sci.* **31** (1996) 1035.
8. M. ALLAHVERDI, R. A. L. DREW and J. STROM OLSEN, *J. Mater. Sci. Eng.* **A207** (1996) 12.
9. M. ALLAHVERDI, Ph.D. Thesis, Department of Mining and Metallurgical Engineering, McGill University, Montreal, Canada (1995).
10. M. ALLAHVERDI, R. A. L. DREW and J. STROM-OLSEN, *Ceram. Eng. Sci. Proc.*, **16** [4–5] (1995) 1015.
11. J. MCKITTRICK, G. KALONJI and T. ANDO, *J. Non-Cryst. Solids* **94** (1987) 163.
12. T. ANDO and Y. SHIOHARA, *J. Amer. Ceram. Soc.* **4** [2] (1991) 410.
13. J. MCKITTRICK, G. KALONJI and T. ANDO, in "Advances in Ceramics", Vol. **24**, "Science and Technology of Zirconia III", edited by S. Somiya, N. Yamamoto and H. Yanagida (The American Ceramic Society Inc., Westerville, OH, 1988) p. 267.
14. N. CLAUSSEN, G. LINDERMANN and G. PETZOW, *Ceram. Int.* **9** [3](1983) p. 83.
15. R. STEVENS, "Zirconia and zirconia ceramics", (Magnesium Elektron Ltd., Twickenham, UK, 1986).
16. Y. ZHOU and T. C. LEI, *J. Amer. Ceram. Soc.* **74** [3] (1991) p. 633.
17. R. CHAIM, P. A. LABUN, V. LANTERI and H. A. HEUER, in "Ceramic Microstructure '86, Materials Science Research", Vol. **21**, edited by J. A. Pask and A. G. Evans (Plenum Press, New York, 1987) p. 203.
18. D. W. RICHERSON, "Modern ceramic engineering" (Marcel Dekker Inc., New York, 1982) p. 745.
19. J. A. PASK, X. W. ZHANG, A. P. TOMSIA and B. E. YOLDAS, *J. Amer. Ceram. Soc.* **70** [10] (1987) 704.
20. T. J. MROZ Jr., and J. W. LAUGHNER, *ibid.* **72** [3] (1989) 508.
21. R. RICE, in "Advanced Ceramic Processing and Technology", edited by J. G. P. Binner (Noyes Publications, Park Ridge, 1990) p. 189.
22. F. F. LANGE, in "Ceramic Microstructure '86, Materials Science Research", Vol. 21, edited by J. A. Pask and A. G. Evans (Plenum Press, New York, 1987) p. 497.
23. W. D. KINGERY, "Introduction to ceramics" (John Wiley and Sons Inc., New York, 1960) p. 265.
24. A. BARONNET, *Fortschr. Miner.* **62** [2] (1984) 187.
25. P. HARTMAN, in "Morphology of crystals: Part A", edited by I. Sunagawa (Perra, Scientific, Tokyo, 1987) p. 367.
26. P. HARTMAN and W. G. PEDROK, *Acta Crystall.* **8** (1995) 49.



*Received 18 October 1995*
*and accepted 8 May 1996*